INTERNATIONAL JOURNAL OF STRUCTURAL CHANGES IN SOLIDS – Mechanics and Applications
Volume 3, Number 3, 2011, pp. 1-19

IJSCS

Studies on effective fiber and matrix poling characteristics of 1-3 piezoelectric composites

M. Sakthivel, A. Arockiarajan*

[a]*Department of Applied Mechanics, Indian Institute of Technology Madras, Chennai 600 036, India.*

Abstract

An analytical model is developed to evaluate the performance of 1-3 piezoelectric composite where both matrix and fiber materials are piezoelectrically active. A parametric study is conducted to investigate the effects of variations in the poling characteristics of the fiber and matrix phase on the overall thermo-electro-mechanical behavior of a 1-3 piezocomposite. The figures of merit (FOM) of the 1-3 composite as a transducer for underwater acoustics and biomedical imaging applications has been analyzed. The proposed model is capable of predicting the effective properties of the composite subjected to thermo-electro-mechanical loading conditions for different poling directions. The predicted variations in the effective elastic, piezoelectric and dielectric material constants are nonlinear in nature for various fiber volume fraction. The influence of thermal effects on effective properties of the composite has been identified. The analytical results show that an appropriate selection of the poling characteristics of the individual fiber and matrix phases could lead to the development of a piezocomposite with significant effective properties

Key words: Pyroelectricity; Thermal effects; Effective properties; Electromechanical coupling factor.

1. Introduction

Piezoelectric materials represent a popular class of active materials which transfer energy between the mechanical domain and electrical domain. Monolithic or bulk Piezoelectric materials have been widely used as actuators and sensors, given their high electromechanical coupled performances. However, bulk piezoelectric materials have certain limitations such as brittle behavior, high acoustic impedance and are very sensitive to cracking; Nelson (2002). Piezoelectric composite materials have been introduced where the bulk piezoelectric material in the form of fibers, is combined with a ductile polymer matrix; refer Newnham *et al.* (1978). Piezoelectric composites have been fabricated in several forms based on fiber and matrix connectivity; for instance (0-3), (1-3) and (2-2). 1-3 piezoelectric ceramic/polymer composites exhibit better characteristics over bulk piezoelectric materials, such as high piezoelectric constant, minor lateral electromechanical coupling, low acoustic impedance, broad bandwidth, and so on; (Uchino (2000), Topolov and Bowen (2009)). Hence, by selecting different piezoelectric ceramics and polymers or different proportions and spatial scales of ceramics, the piezocomposite properties yield better technological solutions then can meet the requirements of some special devices such as medical diagnostic ultrasonic transducers, hydrophones (Klicker *et al.* (1981), Avellaneda and Swart (1998)).

In the literature, several studies have been presented on developing analytical and numerical models for predicting the effective electromechanical response of composites. A simple analytical model is developed by Newnham *et al.* (1978) based on series and parallel connectivity for piezoelectric composites. This model concludes that the composite models can be used for interpreting the properties of a single phase materials as

*Email: aarajan@iitm.ac.in

well as composites. The dilute, self-consistent, Mori-Tanaka (MT) and differential micromechanics theories are extended to predict the effective electromechanical properties of piezoelectric composites and compared with existing experimental data (Dunn and Taya (1993)). An extension of MoriTanaka and Self-consistent approaches are proposed by Odegard (2004). This work offers a comprehensive comparison of the four modeling approaches for a wide range of matrix and reinforcement electromechanical properties, reinforcement geometry and reinforcement volume fraction. Kar-Gupta and Venkatesh (2007) presented an analytical model using the equivalent layer composite model where both the matrix and fiber phases are piezoelectrically active. Recently, the influence of porosity in the polymer matrix as well as passive and active matrix on the performance of 1-3 piezoelectric composites was addressed based on a micromechanics based approach (Della and Shu (2008)). Similarly, several work based on finite element (FE) formulation have been presented on the literature to understand the constitutive behavior of piezoelectric composites wherein the interface effects are addressed; refer Poizat and Sester (1999); Pettermann and Suresh (2005); Berger *et al.* (2007).

The piezocomposites are used in many applications where the impact of thermal effects are in a considerable range and the determination of effective properties is of significant importance under thermal effects Tauchert (1992). Since the usage of piezocomposite under thermal environment is unavoidable in the current status, it is important to study on the effective thermo-electro-mechanical properties on 1-3 piezocomposite. Though determination of effective electro-mechanical properties of 1-3 composite have been reported in the literature, authors are not aware of any published work in determination of effective thermo-electro-mechanical properties of such 1-3 composites (except Kumar and Chakraborty (2009)). Hence, this work focuses on thermo-electro-mechanical coupling studies on composites.

Secondly, the prediction of effective properties on piezoelectric composites are reported in the literature, but there are very few contributions to show what will happen to the effective piezoelectric behavior of the composites if the piezoelectric ceramic PZT rods are not perfectly aligned with the loading direction; refer Fig. 2- Class V material. Nan *et al.* (2000) work focuses on the effective properties of 1-3 type piezoelectric composites with various orientations of lead zirconate titanate rods/fibers aligned in an epoxy matrix using the Green's function technique. Due to manufacturing difficulties, the fiber rod alignment may not be parallel to the loading direction in the 1-3 piezocomposites. This issue motivates us to study the effective properties of composites under different fiber poling direction.

The piezocomposite with two piezoelectric phases (fiber and matrix are active phases) can be used to fabricate novel structure transducers such as two intertwined arrays using the ceramic phase to transmit and using the piezo-polymer matrix to receive. Also, the piezoelectric coefficients of the ceramic and polymer are of opposite signs and significantly different (Taunaumang *et al.* (1994)). But, it may be possible to pole the two phases in opposite directions, that will give enhanced coupling coefficient due to the add-on contribution from active fiber as well as matrix. This problem definition motivates to do the parametric study on the effective properties of composites under different matrix poling directions with respect to fiber directions. By having this three problem in-hand, the overall objectives of the present study are:

1. to develop an analytical model to capture the effective thermo-electro-mechanical response of 1-3 piezoelectric composites where both the fiber and matrix are transversely isotropic and piezoelectrically active.
2. to predict and compare the fundamental elastic, dielectric and piezoelectric material constants of 1-3 piezoelectric composites for different fiber and matrix poling direction.
3. to study the influence of ceramic base volume fraction on the variation of effective thermal and pyroelectric properties.
4. to perform a parameter study to examine the influence of ceramic base volume fraction on the performance of 1-3 type composite for underwater and biomedical imaging transducer applications and compare the performance for 0^0, 90^0, 180^0 and 270^0 matrix poling direction (Class I - IV) and for 0^0, 30^0, 45^0, 60^0 and 90^0 fiber poling direction (Class V); see Fig. 2.

The outline of the paper is as follows: the model formulation is discussed in Section 2 based on the constitutive behavior of piezoelectric composite, assumptions and validity of the model, effective parameter expressions of the 1-3 composite and the performance formulation of 1-3 piezocomposite for fiber and matrix poling directions. Aspects of the related implementation, analytical treatment and numerical examples are discussed in Sections 3. Finally, a short summary concludes the paper, see Section 4.

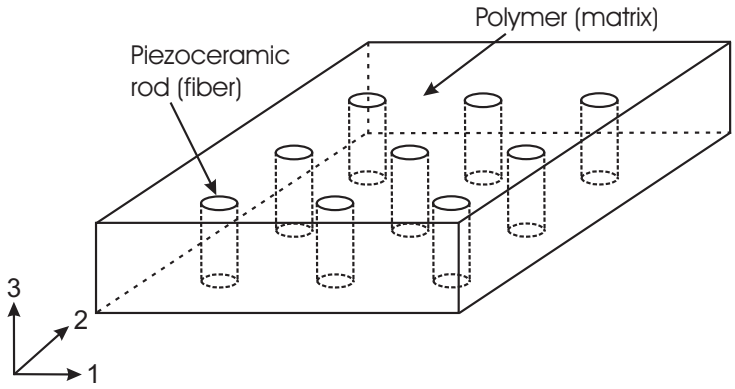

Figure 1: Schematic of a 1-3 piezoelectric composite

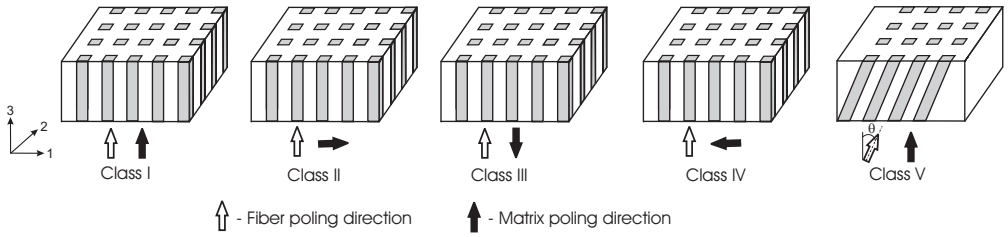

Figure 2: Illustration on classification of 1-3 piezocomposites based on the relative orientation of the poling directions of the fiber and matrix phases (Class I-V)

2. Model formulation

The piezoelectric composite materials can be classified into ten different connectivities, based on the fiber and matrix phases in zero, one, two, or three dimensions Newnham *et al.* (1978). The 1-3 piezoelectric composites consist of the piezoelectric rods (continuous connectivity in one dimension) which are embedded into the active matrix that has continuous connectivity along all three dimensions, refer in fig. 1. Two distinct choices for the poling characteristics of the fiber and matrix phases (poled in a direction parallel to fiber axis, and poled in a direction transverse to the fiber axis) result in four unique piezocomposite classes (Fig. 2), described as follows:

I Fiber and matrix phases are poled in longitudinal directions (both in +3 axis) that are aligned and parallel with the fiber axis.

II Fiber is poled in a longitudinal direction (+3 axis) and matrix phase is poled in a transverse direction (+1 axis).

III Fiber and matrix phases are poled in longitudinal directions (+3 axis and -3 axis) that are aligned and antiparallel with the fiber axis.

IV Fiber is poled in a longitudinal direction (+3 axis) and matrix phase is poled in a transverse direction (-1 axis).

V Fiber is oriented with some angle θ about the longitudinal direction (+3 axis) and matrix phase is poled in a longitudinal direction (+3 axis).

2.1. Constitutive relation of piezoelectric composite

Since the 1-3 composite can be treated as bulk piezoelectric ceramics, they have identical linear constitutive equations as piezoelectrics, which can be written as

$$\begin{aligned} \sigma_{ij} &= C^E_{ijkl}\varepsilon_{kl} - e_{ijk}E_k - \beta_{ij}\theta \\ D_i &= e_{ikl}\varepsilon_{kl} + \kappa^{\varepsilon}_{ij}E_j + P_i\theta \end{aligned} \tag{1}$$

where σ_{ij}, ε_{ij}, E_i and D_i are the stress tensor, stain tensor, electric field vector and electric displacement vector, respectively. C_{ijkl}, e_{ijk}, κ_{ij}, ($\beta_{ij} = C_{ijkl}\,\alpha_{kl}$) and P_i are the elastic stiffness tensor, piezoelectric tensor, permittivity tensor, thermal coefficient tensor, and pyroelectric vector, respectively. θ is the change in temperature. The superscripts E and ε indicate that the elasticity and permittivity constants are determined under the conditions of zero or constant electric field and strain, respectively. Based on the representation of Barnett and Lothe (1997), Della and Shu (2008), Eq. (1) can be represented in a single constitutive relation as

$$\Sigma_{iJ} = E_{iJMR}\, Z_{MR} \tag{2}$$

where

$$\Sigma_{iJ} = \begin{cases} \sigma_{ij} & J = 1,2,3 \\ D_i & J = 4 \end{cases} \tag{3}$$

$$E_{iJMR} = \begin{cases} C_{ijmn} & J,M,R = 1,2,3 \\ e_{nij} & J,R = 1,2,3;\ M = 4 \\ e_{imn} & J = 4;\ M,R = 1,2,3 \\ -\kappa_{in} & J,M = 4;\ R = 1,2,3 \\ -\beta_{ij} & M,R = 4;\ J = 1,2,3 \\ P_i & J,M,R = 4 \end{cases} \tag{4}$$

$$Z_{MR} = \begin{cases} \epsilon_{mn} & M,R = 1,2,3 \\ -E_n & M = 4;\ R = 1,2,3 \\ \theta & M,R = 4 \end{cases} \tag{5}$$

here, the lowercase subscripts are summed over the range of 1-3, whereas the upper case subscripts are the assumed values assigned against the particular variable. 1-3 piezoelectric composite resembles similar to the transversely isotropic piezoelectric constitutive equations, Eq. (2) can be written in matrix form (Voigt's notation) as

$$\left[\begin{array}{c} \sigma^x_{11} \\ \sigma^x_{22} \\ \sigma^x_{33} \\ \sigma^x_{23} \\ \sigma^x_{13} \\ \sigma^x_{12} \\ \hline D^x_1 \\ D^x_2 \\ D^x_3 \end{array}\right] = \left[\begin{array}{cccccc|ccc|c} C^x_{11} & C^x_{12} & C^x_{13} & 0 & 0 & 0 & 0 & 0 & -e^x_{31} & -\beta^x_{11} \\ C^x_{12} & C^x_{11} & C^x_{13} & 0 & 0 & 0 & 0 & 0 & -e^x_{31} & -\beta^x_{22} \\ C^x_{13} & C^x_{13} & C^x_{33} & 0 & 0 & 0 & 0 & 0 & -e^x_{33} & -\beta^x_{33} \\ 0 & 0 & 0 & C^x_{44} & 0 & 0 & 0 & -e^x_{15} & 0 & 0 \\ 0 & 0 & 0 & 0 & C^x_{44} & 0 & -e^x_{15} & 0 & 0 & 0 \\ 0 & 0 & 0 & 0 & 0 & C^x_{66} & 0 & 0 & 0 & 0 \\ \hline 0 & 0 & 0 & 0 & e^x_{15} & 0 & \kappa^x_{11} & 0 & 0 & P^x_1 \\ 0 & 0 & 0 & e^x_{15} & 0 & 0 & 0 & \kappa^x_{11} & 0 & P^x_2 \\ e^x_{31} & e^x_{31} & e^x_{33} & 0 & 0 & 0 & 0 & 0 & \kappa^x_{33} & P^x_3 \end{array}\right] \left[\begin{array}{c} \varepsilon^x_{11} \\ \varepsilon^x_{22} \\ \varepsilon^x_{33} \\ 2\varepsilon^x_{23} \\ 2\varepsilon^x_{13} \\ 2\varepsilon^x_{12} \\ \hline E^x_1 \\ E^x_2 \\ E^x_3 \\ \hline \theta^x \end{array}\right] \tag{6}$$

where the superscript x refers to denote the composite as c, the fiber as f, and the matrix as m.

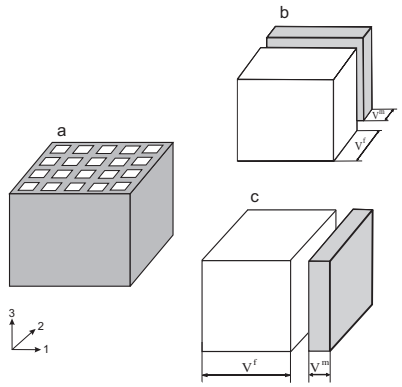

Figure 3: Representation of a 1-3 piezoelectric composite as equivalent layered composite with proportional fiber and matrix volume fractions

2.2. Assumptions and validity of the model

A 1-3 composite is considered to be an equivalent layered composite Hull and Clyne (1996), Kar-Gupta and Venkatesh (2007), Kumar and Chakraborty (2009) where the second phase layer thickness is proportional to the fiber volume fraction. The equivalent series and parallel structure is shown in fig.3. The following assumptions have been employed based on the fundamental concept such as (i) the overall homogenized stress equilibrium condition in the transverse directions (axes -1 and 2), (ii) rule of mixtures concept in the longitudinal direction for stresses (axis-3), and (iii) the homogenized displacement conditions for the longitudinal case in the theoretical calculations (Sakthivel and Arockiarajan (2010)):

In this model, (1) the normal effective stresses along longitudinal direction (axis - 3) and the shear stress in 1-2 plane are predicted based on the individual stress and volume fraction constituents of the fiber and the matrix. (2) The stresses along the transverse directions - 1&2 and the shear stresses in (1-3 & 2-3 planes) are considered to be equal for the fiber, the ceramic and the 1-3 composite, by considering the overall homogeneous stress equilibrium. (3) Concerning the normal effective strain along longitudinal direction and the shear strain in 1-2 plane are considered to be equal for the fiber, the matrix and the 1-3 composite. (4) The effective strain along the transverse directions are the shear strains on the 1-3 & 2-3 planes are calculated based on the individual strain and volume fraction constituents of the fiber and the ceramic. (5) The piezocomposites are dielectric in nature the effective electric displacements along the longitudinal direction can be summed by averaging over the two phases based on a simple theory of series and parallel connectivity. However, the dielectric displacements are taken to be the same in the transverse directions for all. (6) The electric field along the longitudinal direction is considered to be the same for fiber and ceramic and 1-3 composite constituents. Along the other two directions, the electric fields are considered to be zero.

2.3. Effective parameter expressions of the 1-3 composite

The formulation starts with replacing the strain components and electric field of matrix with the fiber and composite strains and electric field based on the assumptions. This calculation gives the strain components and electric field to be only functions of the fiber and the composite. Subsequently, by equating the stress components along the longitudinal direction of ceramic and 1-3 composite, we can get a relation for the fiber strain components in terms of composite strain as well as electric field. Substitution of the derived resulting equation into eq. 6 will thus give the effective electromechanical coefficients of the composite as

$$\begin{aligned}
C_{33}^c &= V^f\left(C_{31}^f A^1 + C_{32}^f B^1 + C_{33}^f + C_{35}^f D^1 - e_{31}^f E^1 - C_{31}^m A^1 - C_{32}^m B^1\right) + C_{33}^m\left(1-V^f\right)\\
\kappa_{33}^c &= V^f\left(e_{31}^f A^2 + e_{32}^f B^2 + \kappa_{33}^f + e_{35}^f D^2 - \kappa_{31}^f E^2 - e_{31}^m A^2 - e_{32}^m B^2\right) + \kappa_{33}^m\left(1-V^f\right)\\
e_{33}^c &= V^f\left(e_{31}^f A^1 + e_{32}^f B^1 + e_{33}^f + e_{35}^f D^1 - \kappa_{31}^f E^1 - e_{31}^m A^1 - e_{32}^m B^1\right) + e_{33}^m\left(1-V^f\right)\\
\beta_{33}^c &= -V^f\left(C_{31}^f A^3 + C_{32}^f B^3 + \beta_{33}^f + C_{35}^f D^3 - e_{31}^f E^3 - C_{31}^m A^3 - C_{32}^m B^3\right) + \beta_{33}^m\left(1-V^f\right)\\
P_3^c &= V^f\left(e_{31}^f A^3 + e_{32}^f B^3 + P_3^f + e_{35}^f D^3 - \kappa_{31}^f E^3 - e_{31}^m A^3 - e_{32}^m B^3\right) + P_3^m\left(1-V^f\right)
\end{aligned} \tag{7}$$

where the required constant A^i, B^i,D^i and E^i can be referred from the Appendix -A. Eq. 7 shows the effective parameter expressions of 1-3 composite with 90^0 degree poling direction of matrix phase (class II material). Similarly, eq. 8 shows the the effective properties for the class V material wherein the fiber rod is rotated with some angle θ from the longitudinal axis.

$$\begin{aligned}
C_{33}^c &= V^f\left(C_{31}^f S^3 + C_{32}^f K^3 + C_{33}^f - C_{31}^m S^3 + C_{32}^m K^3 - e_{32}^m F^3\right) + \left(1-V^f\right) C_{33}^f\\
e_{33}^c &= V^f\left(e_{31}^f S^3 + e_{31}^f K^3 + e_{33}^f - e_{35}^m M^3\right)\\
\kappa_{33}^c &= V^f\left(e_{31}^f S^6 + e_{31}^f K^6 + \kappa_{33}^f - e_{35}^m M^6\right) + \left(1-V^f\right)\kappa_{33}^m\\
\beta_{33}^c &= V^f\left(C_{13}^f S^7 + C_{23}^f K^7 + \beta_{33}^f - C_{13}^m S^7 + C_{23}^m K^7 - e_{13}^m F^7\right) + \left(1-V^f\right)\beta_{33}^m\\
P_3^c &= V^f\left(e_{31}^f S^7 + e_{31}^f K^7 - e_{31}^m S^7 - e_{31}^m K^7 + P_3^f\right) + \left(1-V^f\right) P_3^m
\end{aligned} \tag{8}$$

where the required constant S^i, K^i,and M^i can be referred from the Appendix -B. The performance evaluation of piezoelectric composites for various applications has been discussed in the literature; refer Kar-Gupta and Venkatesh (2007), Della and Shu (2008). Figure of merit help assess the utility of a structure for particular applications. Three important figures of merit - the piezoelectric charge coefficient (d_h), the acoustic impedance (Z), and the coupling constant (K_t) are typically invoked to characterize the utility of piezocomposite in practical applications.

3. Results and discussion

The effective properties of the proposed 1-3 piezocomposite material for different fiber and matrix poling directions are calculated using the model derived in the previous section. In the present work, the fiber(rod) is chosen as TLZ-5, and the matrix is VDF/TrFE copolymer that possess high value of piezoelectric and pyroelectric coefficients when compared to other polymer materials. Table 1 shows the material parameters of the ceramic (fiber) and copolymer (matrix) that are used in the calculations. In the calculations, $(\cdot)^f$ and $(\cdot)^m$ are referred to the parameters of TLZ-5 material and VDF/TrFE copolymer parameters. This work focuses on capturing the effect of ceramic rod volume fractions on mechanical, electrical and thermal characteristics of the 1-3 piezocomposite materials. The results are discussed into two parts, namely: effective properties of 1-3 composite due to matrix orientation and variation of composite properties due to fiber orientation.

In order to validate the proposed model, the simulated results are compared with other approaches. Fig. 4 (left) shows the variation of stiffness constant (C_{11}) with fiber volume fraction. The simulated results are compared with the numerical approach Srihari (2011) in which the interface effects are considered and also compared with multiscale approach proposed by Nan *et al.* (2000). The graphs show that the model is in good agreement with the other approaches for most of the values and the percentage deviation lies between $10-15\%$. Similarly, Fig. 4 (right) shows the variation of acoustic impedance (Z) with fiber volume fraction and compared with other approaches as well as experimental data from literature Taunaumang *et al.* (1994). The graphs are in comparable agreement with the experimental data and the percentage of variation is upto 20%. Such deviations may be attributed due to the grain boundry effects and the distribution of fiber. In this model, the interface effects are not considered. However, further research will be focussed in this context.

Table 1: Parameters of the fiber and matrix used in the model calculations (Taunaumang *et al.* (1994))

Parameter	TLZ	VDF/TrFE
C_{11}^E (GPa)	126	8.5
C_{12}^E (GPa)	79.5	3.6
C_{13}^E (GPa)	84.1	3.6
C_{33}^E (GPa)	109	9.9
C_{33}^D (GPa)	147	10.7
C_{44}^E (GPa)	23	1.9
C_{66}^E (GPa)	23.5	2.45
e_{15} (C/m^2)	17	-0.002
e_{31} (C/m^2)	-6.5	0.008
e_{33} (C/m^2)	24.8	-0.29
$\kappa_{11}^{\varepsilon}, \kappa_{22}^{\varepsilon}$ (C/Vm)	1.505 x 10^{-8}	6.641 x 10^{-11}
$\kappa_{33}^{\varepsilon}$ (C/Vm)	1.605 x 10^{-8}	7.960 x 10^{-11}
$\alpha_{11}, \alpha_{22}, \alpha_{33}$ $(^{\circ}C^{-1})$	1.2 x 10^{-6}	0.18 x 10^{-6}
P_1, P_2, P_3 $(C/K/m^2)$	2.5 x 10^{-5}	2.0 x 10^{-5}
ρ (kg/m^3)	7898	1880

3.1. Effective thermo-electro-mechanical properties – Matrix rotation

The rods are aligned along the direction - 3. For class I type composites, the fiber and the matrix are poled along the same direction. However, the composites that belong to classes II and IV (90^0 and 180^0), the material properties of matrix have been rotated appropriately. In the subsequent discussions, the results of class IV materials are not presented, since the class II and IV materials have an identical results. In general, the sensitivity of transducers are measured based on the electro-mechanical coefficient (refers to energy conversion between mechanical to electrical and vice-versa). It is desired to have larger coupling constants being more desirable. The operating bandwidth of the devices can be determined by using the electromechanical coupling constant (K_t). The variation of effective electromechanical coupling constant (K_t) for the 1-3 type piezocomposite with respect to the volume fraction of fiber rods (V^f) for different poling direction of matrix (class I-IV) is shown in fig. 5. The electro-mechanical coefficient increases gradually as volume fraction of fiber increases due to the fact that the electrical energy is more conveniently converted into the mechanical energy. As the high end of fiber volume fraction approaches, the K_t value reduces towards the value of fiber due to lateral clamping of the fiber by the polymer. At the medium range of ceramic rod volume fraction ($0.2 < V_1 < 0.8$), K_t value is almost a constant value. It is desired to have larger coupling constants being more desirable for the design aspects. In this context, it shows that the maximum K_t value can be achieved between 40 to 80 % fiber volume fraction. K_t value is unaffected by the different matrix poling directions.

The acoustic impedance (Z) is an important parameter for the determination of acoustic transmission and reflection at the boundary of two materials having different acoustic impedances. In order to enhance the performance of the transducer, good impedance matching between the transducer and the surrounding media (e.g., water, human tissue) is desired. The bulk piezoceramic materials typically have higher acoustic impedance than the surrounding environment. For instance, the acoustic impedance of a piezoceramic transducer is around 30 MRayl, while the surrounding environment (blood or soft tissue) is in the order of 1.5 MRayl. The impedance parameter can be significantly enhanced by appropriate design of a composite structure, that renders the development of piezoelectric polymer materials such as PVDF opened up the new possibilities for transducers operating at low acoustic impedance. The acoustic impedance of piezocomposite materials can vary in the order of 10 MRayl. Fig. 6 demonstrates that combination of good acoustic properties can be achieved by making optimal selection of ceramic rod volume fraction. It also shows that the acoustic impedance increases linearly as the volume fraction of fiber increases except for some deviations at the high fiber volume fraction. For the different kind

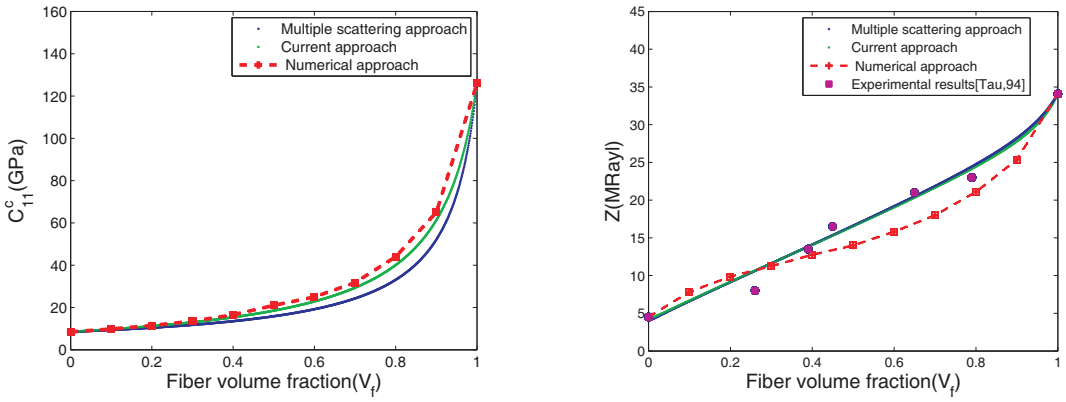

Figure 4: (left) Variation of stiffness constant (C_{11}) with the ceramic rod volume fraction (V^f); (Right) Variation of acoustic impedance (Z) with the ceramic rod volume fraction (V^f) – Srihari (2011)

of poling directions of matrix (class I- IV), the impedance properties do not have much variations. The essential requirement for designing a transducer is the low acoustic impedance and the high electro-mechanical coupling coefficient. From the designer prospective; the requirement of impedance for underwater and bio-medical imaging applications are in the order of 2 to 12 MRayl. This requirement can be achieved by 10 to 20 % fiber volume fraction but different matrix poling direction do not have any impact on the impedance values. The present study shows that 1-3 composites can be superior in both aspects such as minimizing impedance and maximizing coupling factor.

The effectiveness of piezocomposite for the hydrophone applications can be represented by the hydrostatic piezoelectric coefficient, and hydrostatic voltage coefficient. d_h captures the effective strength of the electro-mechanical coupling in a piezoelectric material, esp., in the conversion of hydrostatic mechanical loads to electrical signals. In applications such as in hydrophones, large values of the piezoelectric charge co-efficient is desirable in order to achieve sensitivity to the detection of sound waves. Fig. 7 shows the effective hydrostatic charge coefficient (d_h) of the piezoelectric composite with respect to the volume fraction of the ceramic rod. The pattern of curve shows that the charge coefficient of 1-3 type composite decreases as the ceramic rod volume fraction (V^f) increases over 30%. It is also observed that this coefficient is very high at low ceramic rod volume fraction for 90^0 degree poling direction compared with 0^0, and 180^0 degree poling directions. From design consideration, the maximum d_h can be achieved around 30% of fiber volume fraction with 0^0, and 180^0 degree poling directions. With 90^0 matrix poling direction, there is a steep increase and decrease behavior and may not fit for optimized design.

The design of 1-3 piezocomposite for underwater application is focused on the hydrostatic pressure response – figure of merit (FOM) that needs to be maximized ($d_h g_h$) by varying the matrix and fiber material properties, and fiber volume fraction. Owing to the improvements in their d_h and g_h values, the 13 type samples had high FOM values. The effective hydrophone figure of merit (FOM) is plotted as a function of ceramic rod volume fractions in fig. 8, wherein this value does not deviate much for Class I and III materials. However, FOM varies significantly when the poling of matrix is at 90^0. Since FOM is direct product of d_h and g_h, the maximum FOM can be achieved around 30% of fiber volume fraction with 0^0, and 180^0 degree poling directions. With 90^0, and 270^0 matrix poling direction, there is a steep increase and decrease behavior which might not sutiable for tansducer applications.

The piezocomposites are used as transducer in the active structures which are subjected to thermal environments. Hence, the transducer material should have high heat resistance, strength and stiffness in order to withstand the thermal impacts. When the 1-3 piezoelectric materials are exposed to thermal loads, they exhibits pyroelectric effect and generates temporary electric charges due to the thermal strain. This effect can also be used for applications like infrared detector, pyrometer, and energy harvesting, etc. A new pyro-electric material

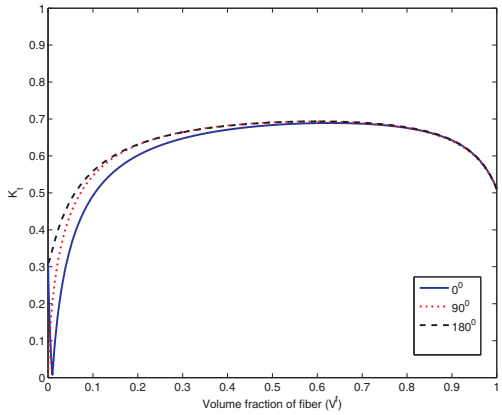

Figure 5: Variation of electromechanical coupling constant (K_t) with the ceramic rod volume fraction (V^f)

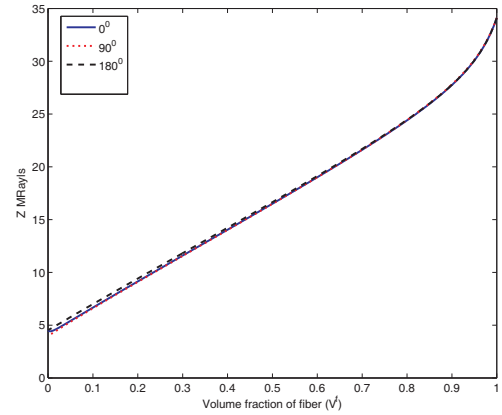

Figure 6: Variation of acoustic impedance (Z) with the ceramic rod volume fraction (V^f)

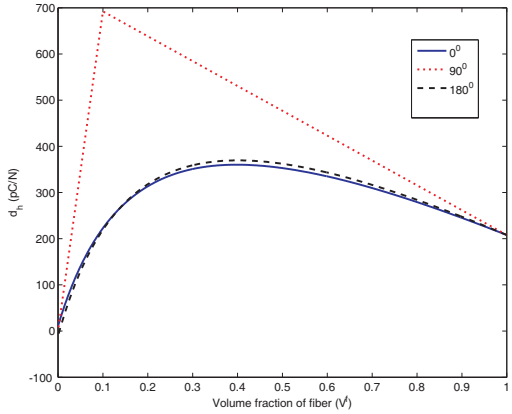

Figure 7: Variation of hydrostatic charge constant (d_h) with the ceramic rod volume fraction (V^f)

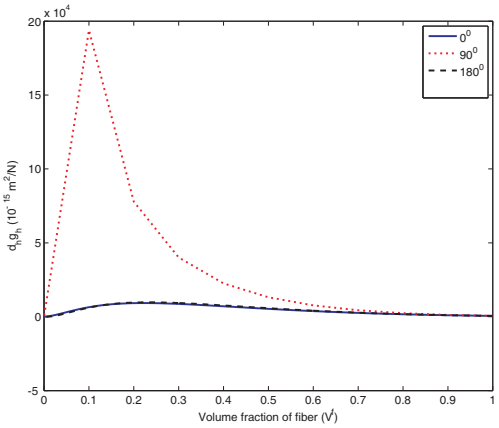

Figure 8: Variation of hydrostatic figure of merit ($d_h g_h$) with the ceramic rod volume fraction (V^f)

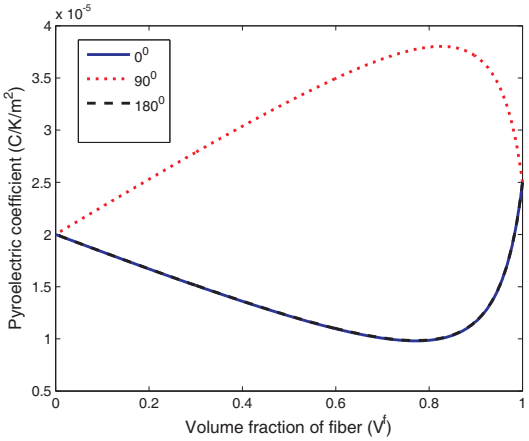

Figure 9: Variation of pyroelectric coefficient (P_3) with the ceramic rod volume fraction (V^f)

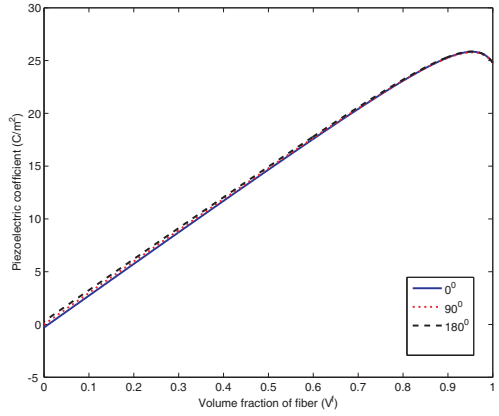

Figure 10: Variation of piezoelectric coefficient (e_{33}) with the ceramic rod volume fraction (V^f)

can be tailored by combining the bulk ceramic and polymer phase with appropriate proportions and properties. The plot shows the non-linear variation of pyroelectric coefficient in longitudinal direction (P_3) for class I and III type materials (Fig. 9). The pyroelectric coefficient decreases up to the ceramic rod volume fraction of around 80% due to the domination of the matrix coefficient over the fiber value. The piezoelectric coupling coefficient is directly proportional to the electrical to acoustic conversion that determines the transducer efficiency. Linear variation is noticed in Fig. 10 for most of the volume fraction of the fiber but there is a minimal decrease in the value at high fiber volume fraction.

3.2. Effective thermo-electro-mechanical properties – Fiber rotation

This section concentrates on analyzing the effective properties of the 1-3 composite with respect to the different fiber poling direction. Fig. 11 shows the non-linear variation of the electromechanical coupling coefficient (K_t) for various fiber poling directions as a function of the fiber volume fraction. As the orientation of the fiber rods deviates from the 3 - axis, i.e. $\theta > 0$, there is a significant reduction in the (K_t) value irrespective of fiber volume fraction. It is desired to have larger coupling constants being more desirable for the design aspects. However, different fiber poling direction gives reduction in the K_t values. Hence, it is not desirable to use different fiber orientation for transducer design. The acoustic impedance (Z) shown in Fig. 12 is a useful parameter for biomedical imaging application and the predicted results shows that the acoustic impedance increases linearly as the volume fraction of the fiber increases except for some deviations at the high fiber volume fraction. The variations of acoustic impedance between the different fiber poling directions are minimal. From the designer prospective; the requirement of impedance for underwater and bio-medical imaging applications are in the order of 2 to 12 MRayl.

Fig. 13 shows the effective hydrostatic charge coefficient (d_h) of the piezoelectric composite with respect to the volume fraction of the ceramic rod. The pattern of curve shows that the charge coefficient of 1-3 type composite decreases as the ceramic rod volume fraction (V_1) increases over 35% for the poling angle $\theta = 0$. However, the orientation of the fiber rods deviates from the 3 - axis, i.e. $\theta > 0$, this value decreases at high fiber volume fraction. The effective hydrophone figure of merit (FOM) as a function of ceramic rod volume fractions is shown in fig. 14. The variation in FOM is direct consequence of d_h and g_h since it is the direct product of d_h and g_h. FOM is direct product of d_h and g_h and the maximum FOM can be achieved around 90% of fiber volume fraction with 30^0 degree poling directions. With 60^0, and 90^0 fiber poling direction, FOM effect is negligible and might not sutiable for tansducer applications. The plot shows the non-linear variation of pyroelectric coefficient in longitudinal direction (P_3) for different fiber poling directions (Fig. 15). The pyroelectric coefficient decreases up to the ceramic rod volume fraction of around 80% due to the domination of the matrix coefficient value over the fiber value except perpedicular fiber poling direction ($\theta = 90^0$). If the poling direction of fiber deviates from $\theta = 90^0$ then at high fiber volume fraction this constant decreases. The coupling coefficient (e_{33}) varies linearly with volume fraction over most of the range (Fig. 16). With different fiber poling direction, the (e_{33})value is almost same.

3.3. Optimal design problem

This section begin with a description of the design parameters for transducer design using 1-3 piezocomposite. The following parameters are considered as:

I **Volume fraction of the PZT rods:** All of the properties of the composite are very sensitive to the volume fraction of the PZT rods and hence it is one of the main design variables of the problem.

II **Arrangement of the PZT rods:** Piezoelectric composite materials are transversely isotropic in nature. Given the properties and volume fractions of the PZT rods and the matrix, the hydrophone characteristics are uniquely defined by the effective transverse bulk modulus that depends on the spatial arrangement of the PZT rods. Hence the hydrophone performance characteristics are determined by the influence of the shape and distribution of the rod.

III **Properties of the matrix:** The hydrophone characteristics are very sensitive to the properties of the matrix material. Avellaneda and Swart (1994) showed that introducing additional porosity into the isotropic polymer matrix may dramatically improve the performance of the composite. It is also reported that

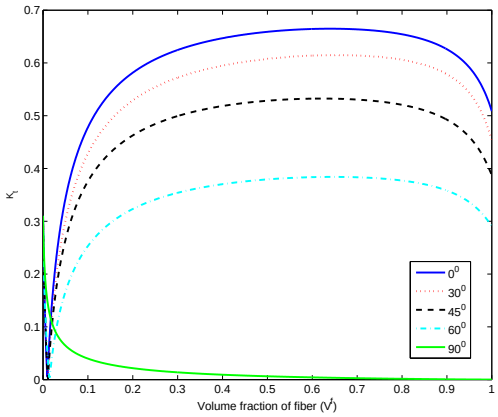

Figure 11: Variation of electromechanical coupling constant (K_t) with the ceramic rod volume fraction (V^f)

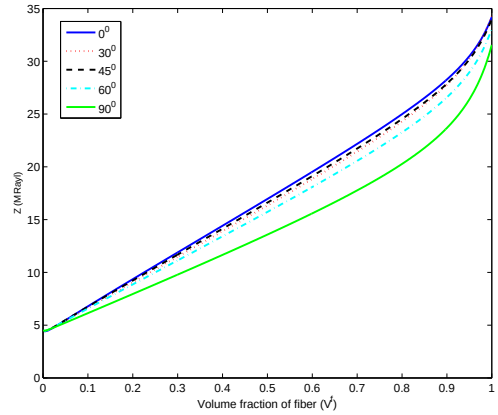

Figure 12: Variation of acoustic impedance (Z) with the ceramic rod volume fraction (V^f)

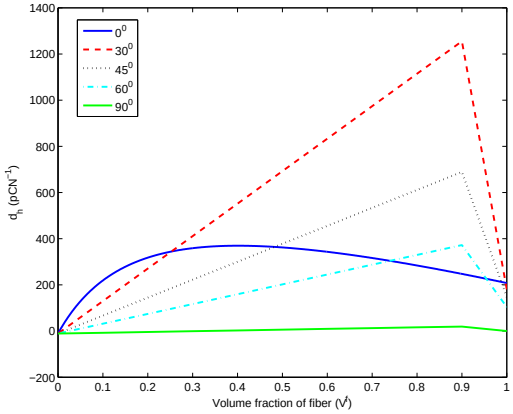

Figure 13: Variation of hydrostatic charge constant (d_h) with the ceramic rod volume fraction (V^f)

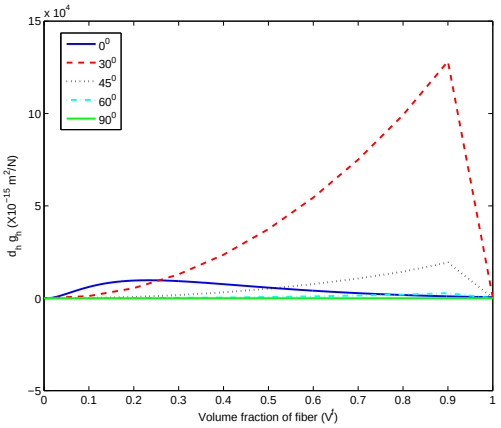

Figure 14: Variation of hydrostatic figure of merit ($d_h g_h$) with the ceramic rod volume fraction (V^f)

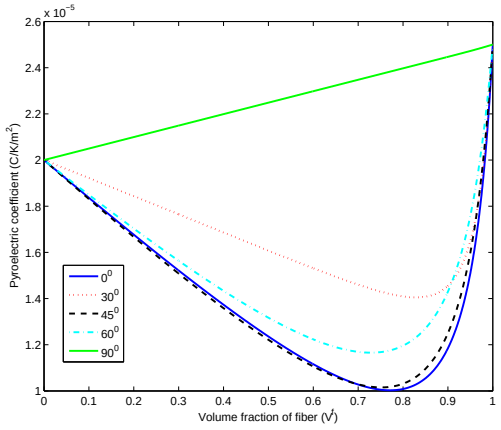

Figure 15: Variation of pyroelectric coefficient (P_3) with the ceramic rod volume fraction (V^f)

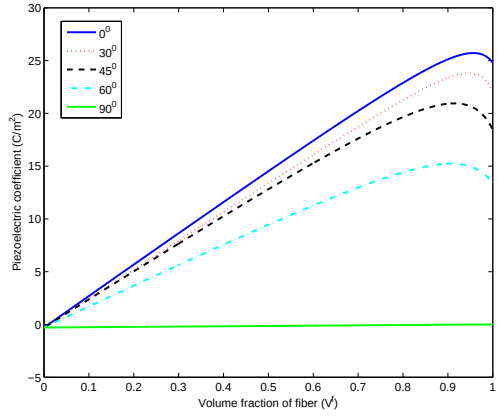

Figure 16: Variation of piezoelectric coefficient (e_{33}) with the ceramic rod volume fraction (V^f)

decreasing the Poisson's ratio of the matrix may result in enhanced performance of the composite. It is important to explore the idea of optimally designing the matrix for the piezoelectric composite.

IV **Properties of the piezoceramic fibers:** The moduli, dielectric constant of the piezoceramic rod is very important that should combine with the polymer on order to get the enhanced properties.

V **Fiber poling directions:** Due to manufacturing difficulties, the fiber rod alignment may not be parallel to the loading direction in the 1-3 piezocomposites. This manufacturing issue can be considered for optimal design.

VI **Matrix poling directions:** Since the piezoelectric coefficients of the ceramic and polymer are of opposite signs and significantly different, it may be possible to pole the two phases in opposite directions, that will give enhanced coupling coefficient due to the add-on contribution from active fiber as well as matrix. This idea can be incorporated for design considerations.

Having defined the optimal design parameters, the effective transducer (hydrophone and bio-medical application) performance coefficients can be maximized based on the following functionals:

1 The electromechanical coupling constant (K_t)
2 The acoustic impedance (Z)
3 The longitudinal velocity (V_{33}^D)
4 The effective hydrostatic charge coefficient (d_h)
5 The effective hydrostatic voltage coefficient (g_h)
6 A common hydrostatic figure of merit - FOM ($d_h \cdot g_h$)
7 The effective electromechanical coupling factor (k_h)

In this work, the above mentioned optimal parameters and the effective transducer performance functionals are being calculated using the layered approach (refer sec. 2.3) and the simulated results are discussed in detail in section 3. Additionally the predicted performance functional variations for different fiber and matrix poling direction are tabulated; see Tables. 2 and 3 .

Based on the previous discussion, the performance coefficients can be predicted in terms of the volume fraction of the piezoelectric rods and the fiber, matrix poling directions.

Based on the problem in hand, we can optimize the possible combination to get the enhanced properties for transducer application. Consider a case study wherein the requirement is to maximize the hydrostatic charge coefficient (d_h), the hydrostatic voltage coefficient (g_h) and the Figure of Merit (FOM). The fiber and matrix material properties are used from the table 1 for this analysis and the optimum solution can be achieved for 20 to 30 % of fiber voulme fraction. Concerning the different poling directions, it is appreciable to use 0^0 and 180^0 matrix poling directions. The other possible matrix and fiber poling directions cannot fit the requirment due to the significant variations with respect to fiber volume fraction. From this study, the design procedure is suggested as follows:

1 Take a fiber and matrix material, described by a individual properties and an equivalent layered model;
2 Find the effective material properties for piezocomposites based on the fiber volume fraction using the proposed layered approach;
3 Find the effective piezocomposite properties as functions fiber and matrix poling directions;
4 Find the hydrophone and bio-medical performance coefficients;
5 Find optimal volume fraction (V^f) by performing the optimization procedure until convergence;
6 Perform sensitivity analysis (with respect to fiber volume fraction);
7 Change volume fraction and poling directions using optimization technique;
8 Go to step 2 (repeat until convergence).

Table 2: Variations of performance parameters for different matrix poling direction

[1ex] V^f	Angle	K_t	Z $(MRayl)$	V_{33}^D $\times 10^3$ (m/s)	d_h (pC/N)	g_h $(mV.m/N)$	FOM $\times 10^3$ (p/Pa)	k_h	P_3 $\times 10^{-5}$ C/K/m^2	β_{33} $\times 10^5$ N/m^2/^0C
1	0^0	0.510	34.1	4.31	208	26.9	.56	0.17	2.5	3.3
	90^0	0.510	34.1	4.31	208	26.9	.56	0.50	2.5	3.3
	180^0	0.510	34.1	4.31	208	26.9	.56	0.17	2.5	3.3
0.9	0^0	0.643	27.7	3.80	245	40.8	1.0	0.20	1.17	1.40
	90^0	0.640	27.8	3.81	262	46.6	1.2	0.34	3.71	1.43
	180^0	0.643	27.7	3.80	247	41.7	1.0	0.20	1.17	1.40
0.8	0^0	0.675	24.4	3.64	280	59.4	1.6	0.23	0.98	9.18
	90^0	0.675	24.4	3.65	315	75.9	2.4	0.34	3.80	9.37
	180^0	0.675	24.4	3.65	284	61.5	1.7	0.23	0.99	9.18
0.7	0^0	0.687	21.6	3.54	309	83.2	2.5	0.26	1.01	6.75
	90^0	0.689	21.6	3.54	369	118	4.3	0.38	3.68	6.87
	180^0	0.690	21.6	3.56	316	863.9	2.7	0.26	1.01	6.75
0.6	0^0	0.688	19.0	3.46	334	113	3.8	0.29	1.01	5.19
	90^0	0.693	19.0	3.46	423	181	7.6	0.45	3.50	5.25
	180^0	0.693	19.1	3.48	343	119	4.0	0.30	1.10	5.19
0.5	0^0	0.683	16.5	3.37	352	150	1.5	0.32	1.22	4.03
	90^0	0.690	16.4	3.37	477	275	7.6	0.32	3.28	4.06
	180^0	0.690	16.6	3.40	362	362	4.0	0.33	1.22	4.03
0.4	0^0	0.67	14.0	3.36	360	196	7.1	0.36	1.43	3.11
	90^0	0.68	14.0	3.32	531	425	2.3	1.05	3.06	3.17
	180^0	0.68	14.2	3.30	370	206	7.6	0.37	1.43	3.11
0.3	0^0	0.65	11.6	3.14	351	246	8.7	0.40	1.51	2.29
	90^0	0.66	11.5	3.14	585	686	4.0	1.09	2.79	2.29
	180^0	0.66	11.8	3.21	359	258	9.3	0.40	1.51	2.29
0.2	0^0	0.60	9.14	2.96	313	292	9.2	0.42	1.67	1.58
	90^0	0.63	9.09	2.95	638	968	7.8	0.64	2.53	1.56
	180^0	0.63	9.41	3.05	318	292	9.6	0.42	1.67	1.58
0.1	0^0	0.49	6.66	2.68	223	288	6.4	0.40	1.83	9.20
	90^0	0.55	6.59	2.66	692	1100	1.9	0.50	2.27	9.00
	180^0	0.56	6.99	2.82	219	279	6.4	0.40	1.83	9.20
0.0	0^0	0.31	4.54	2.41	-11	14.7	-1.6	0.09	2.00	3.08
	90^0	0.22	4.00	2.13	0	0	0.9	0.00	2.00	2.83
	180^0	0.31	4.54	2.41	-11	14.7	-1.6	0.09	2.00	3.08

Table 3: Variations of performance parameters for different fiber poling direction

V^f	Angle	K_t	Z $(MRayl)$	V_{33}^D $\times 10^3$ (m/s)	d_h (pC/N)	g_h $(mV.m/N)$	FOM $\times 10^3$ (p/Pa)	k_h	P_3 $\times 10^{-5}$ C/K/m^2	β_{33} $\times 10^5$ N/m^2/^0C
1	0^0	0.51	34.1	4.32	208	26.9	.56	0.17	2.5	3.3
	30^0	0.46	30.5	3.86	180	20.6	.37	0.05	2.5	3.3
	45^0	0.39	33.8	4.29	147	13.9	.20	0.04	2.5	3.4
	60^0	0.30	33.0	4.17	104	7.07	.73	0.03	2.5	3.4
	90^0	0.00	31.5	3.99	0	0	0	0	2.5	3.5
0.9	0^0	0.64	27.8	3.80	245	40.8	1.00	0.20	1.2	1.4
	30^0	0.58	22.6	3.10	1255	1021	1.28	0.15	1.5	1.5
	45^0	0.49	24.2	3.33	689	280	1.93	0.11	1.3	1.6
	60^0	0.36	26.6	3.64	372	74	2.77	0.07	1.4	1.7
	90^0	0.00	23.7	3.25	19.5	0	3.71	0	2.4	1.5
0.8	0^0	0.68	24.4	3.65	279	59.4	1.66	0.23	1.0	0.9
	30^0	0.61	19.3	2.89	1144	889	9.92	0.20	1.4	1.0
	45^0	0.52	21.0	3.11	611	235	1.44	0.13	1.0	1.1
	60^0	0.38	23.3	3.47	329	60	1.99	0.07	1.2	1.2
	90^0	0.00	20.3	3.03	16.5	0	2.15	0	2.4	0.9
0.7	0^0	0.69	21.6	3.55	309	83	2.58	0.26	1.0	0.6
	30^0	0.61	19.9	2.78	973	770	7.50	0.22	1.5	0.8
	45^0	0.53	18.4	3.02	533	200	1.07	0.13	1.0	0.9
	60^0	0.38	20.5	3.37	287	50	1.44	0.07	1.2	0.9
	90^0	0.00	17.7	2.92	12.8	0	1.17	0	2.3	0.7
0.6	0^0	0.69	19.0	3.46	334	113	3.80	0.30	1.1	0.5
	30^0	0.61	14.9	2.71	833	654	5.45	0.23	1.5	0.6
	45^0	0.53	16.2	2.95	455	467	7.65	0.13	1.1	0.7
	60^0	0.38	18.1	3.29	244	41	1.01	0.07	1.2	0.7
	90^0	0.00	15.6	2.84	9.4	0	0.05	0	2.3	0.5
0.5	0^0	0.68	16.5	3.38	352	150	5.32	0.33	1.2	0.4
	30^0	0.61	12.9	2.65	692	540	3.74	0.23	1.6	0.5
	45^0	0.53	14.1	2.88	378	137	5.18	0.12	1.2	0.5
	60^0	0.38	15.7	3.22	202	33	0.67	0.06	1.3	0.5
	90^0	0.01	13.6	2.78	6.0	0	0.01	0	2.2	0.4
0.4	0^0	0.67	14.0	3.27	360	195	0.70	0.36	1.4	0.3
	30^0	0.59	11.7	2.60	551	427	2.36	0.21	1.7	0.3
	45^0	0.52	12.1	2.82	300	107	3.22	0.11	1.4	0.4
	60^0	0.37	13.4	3.13	159	25	0.04	0.05	1.4	0.4
	90^0	0.01	11.6	2.72	2.7	0	0.01	0	2.2	0.3
0.3	0^0	0.65	11.6	3.14	351	246	0.86	0.40	1.4	0.2
	30^0	0.57	9.4	2.55	411	314	1.29	0.18	1.8	0.2
	45^0	0.50	10.1	2.75	222	77	0.73	0.09	1.5	0.2
	60^0	0.35	11.1	3.02	117	18	0.02	0.04	1.6	0.3
	90^0	0.01	9.7	2.66	0.7	0	0.01	0	2.1	0.2
0.1	0^0	0.49	6.66	2.68	222	288	0.64	0.40	1.8	0.09
	30^0	0.43	6.00	2.42	130	91	0.11	0.10	1.9	0.05
	45^0	0.38	6.25	2.52	67	21	0.01	0.05	1.8	0.07
	60^0	0.25	6.57	2.65	32	4	0.01	0.02	1.8	0.07
	90^0	0.04	6.13	2.47	-7.1	0	0.00	0	2.1	0.04

4. Summary

In this work, an analytical method based on parallel and series theory has been devised for 1-3 piezoelectric composites. The performance of these composites as transducers for underwater and biomedical applications has been studied. The model is used to calculate the complete effective behavior of the piezoelectric composite subjected to combined thermo-electro-mechanical loading conditions. The effects of variations in the material properties under different fiber and matrix poling directions were studied. It is observed that the variations in the elastic, piezoelectric and dielectric material constants with ceramic rod volume fraction are nonlinear. The analytical study shows that an appropriate selection of the poling characteristics of the individual fiber rod and matrix phases could lead to the development of a piezocomposite for specific devices. The significant variations on effective figures of merit (FOM) were evaluated for ceramic rod volume fraction and poling characteristics on the performance of active 1-3 piezocomposites in bio-medical and underwater applications.

5. Appendix - A

$$
\begin{aligned}
A^1 &= \left(1-V^f\right)\left(A\left(C_{13}^m-C_{13}^f\right)+B\left(C_{23}^m-C_{23}^f\right)-C_{35}^f C-De_{13}^f\right)\\
A^2 &= \left(1-V^f\right)\left(-A\left(e_{13}^m-e_{13}^f\right)-B\left(e_{23}^m-e_{23}^f\right)-Ce_{35}^f-D\kappa_{13}^f\right)\\
A^3 &= \left(1-V^f\right)\left(-A\left(\beta_{11}^m-\beta_{11}^f\right)-B\left(\beta_{22}^m-\beta_{22}^f\right)+D\left(P_1^m-P_1^f\right)\right)\\
B^1 &= \left(1-V^f\right)\left(B\left(C_{13}^m-C_{13}^f\right)+E\left(C_{23}^m-C_{23}^f\right)-C_{35}^f F-Ge_{13}^f\right)\\
B^2 &= \left(1-V^f\right)\left(-B\left(e_{13}^m-e_{13}^f\right)-E\left(e_{23}^m-e_{23}^f\right)-Fe_{35}^f-G\kappa_{13}^f\right)\\
B^3 &= \left(1-V^f\right)\left(-B\left(\beta_{11}^m-\beta_{11}^f\right)-E\left(\beta_{22}^m-\beta_{22}^f\right)+G\left(P_1^m-P_1^f\right)\right)\\
D^1 &= \left(1-V^f\right)\left(C\left(C_{13}^m-C_{13}^f\right)+F\left(C_{23}^m-C_{23}^f\right)-C_{35}^f K-Me_{13}^f\right)\\
D^2 &= \left(1-V^f\right)\left(-C\left(e_{13}^m-e_{13}^f\right)-F\left(e_{23}^m-e_{23}^f\right)+Ke_{35}^f+M\kappa_{13}^f\right)\\
D^3 &= \left(1-V^f\right)\left(-C\left(\beta_{11}^m-\beta_{11}^f\right)-F\left(\beta_{22}^m-\beta_{22}^f\right)+M\left(P_1^m-P_1^f\right)\right)\\
E^1 &= \left(1-V^f\right)\left(-D\left(C_{13}^m-C_{13}^f\right)-G\left(C_{23}^m-C_{23}^f\right)+C_{35}^f M-Ne_{13}^f\right)\\
E^2 &= \left(1-V^f\right)\left(D\left(e_{13}^m-e_{13}^f\right)+G\left(e_{23}^m-e_{23}^f\right)+Me_{35}^f+N\kappa_{13}^f\right)\\
E^3 &= \left(1-V^f\right)\left(D\left(\beta_{11}^m-\beta_{11}^f\right)+G\left(\beta_{22}^m-\beta_{22}^f\right)+N\left(P_1^m-P_1^f\right)\right)\\
Q_1 &= \left[\left(1-V^f\right)\kappa_{22}^f+\left(V^f\kappa_{22}^m\right)\right]\left[\left(1-V^f\right)\kappa_{22}^f+\left(V^f\kappa_{22}^m\right)\right]+\left[\left(1-V^f\right)e_{24}^f+\left(V^f e_{24}^m\right)\right]^2 \qquad (9)\\
A &= \frac{[Q_1]\left\{\left(1-V^f\right)C_{11}^f+\left(V^f C_{11}^m\right)\right\}}{\left[(1-V^f)C_{22}^f+V^f C_{22}^m\right]\left[(1-V^f)C_{55}^f+V^f C_{55}^m\right]\left[(1-V^f)\kappa_{11}^f+V^f\kappa_{11}^m\right]}\\
B &= \frac{[Q_1]\left\{\left(1-V^f\right)C_{12}^f+\left(V^f C_{12}^m\right)\right\}}{\left[(1-V^f)C_{22}^f+V^f C_{22}^m\right]\left[(1-V^f)C_{55}^f+V^f C_{55}^m\right]\left[(1-V^f)\kappa_{11}^f+V^f\kappa_{11}^m\right]}\\
C &= \frac{[Q_1]\left\{\left(1-V^f\right)C_{15}^f\right\}}{\left[(1-V^f)C_{22}^f+V^f C_{22}^m\right]\left[(1-V^f)C_{55}^f+V^f C_{55}^m\right]\left[(1-V^f)\kappa_{11}^f+V^f\kappa_{11}^m\right]}\\
D &= \frac{[-Q_1]\left\{\left(1-V^f\right)e_{11}^f\right\}}{\left[(1-V^f)C_{22}^f+V^f C_{22}^m\right]\left[(1-V^f)C_{55}^f+V^f C_{55}^m\right]\left[(1-V^f)\kappa_{11}^f+V^f\kappa_{11}^m\right]}\\
E &= \frac{[Q_1]\left\{\left(1-V^f\right)C_{55}^f+\left(V^f C_{55}^m\right)\right\}}{\left[(1-V^f)C_{22}^f+V^f C_{22}^m\right]\left[(1-V^f)C_{55}^f+V^f C_{55}^m\right]\left[(1-V^f)\kappa_{11}^f+V^f\kappa_{11}^m\right]}\\
F &= \frac{[-Q_1]\left\{\left(1-V^f\right)e_{15}^f+\left(V^f e_{15}^m\right)\right\}}{\left[(1-V^f)C_{22}^f+V^f C_{22}^m\right]\left[(1-V^f)C_{55}^f+V^f C_{55}^m\right]\left[(1-V^f)\kappa_{11}^f+V^f\kappa_{11}^m\right]}\\
K &= \frac{[-Q_1]\left\{\left(1-V^f\right)e_{33}^f\right\}}{\left[(1-V^f)C_{22}^f+V^f C_{22}^m\right]\left[(1-V^f)C_{55}^f+V^f C_{55}^m\right]\left[(1-V^f)\kappa_{11}^f+V^f\kappa_{11}^m\right]}\\
G &= \frac{[-Q_1]\left\{\left(1-V^f\right)e_{24}^f+\left(V^f e_{24}^m\right)\right\}}{\left[(1-V^f)C_{22}^f+V^f C_{22}^m\right]\left[(1-V^f)C_{55}^f+V^f C_{55}^m\right]\left[(1-V^f)\kappa_{11}^f+V^f\kappa_{11}^m\right]}\\
M &= \frac{[Q_1]\left\{\left(1-V^f\right)\kappa_{11}^f+\left(V^f\kappa_{11}^m\right)\right\}}{\left[(1-V^f)C_{22}^f+V^f C_{22}^m\right]\left[(1-V^f)C_{55}^f+V^f C_{55}^m\right]\left[(1-V^f)\kappa_{11}^f+V^f\kappa_{11}^m\right]}\\
N &= \frac{[Q_1]\left\{\left(1-V^f\right)\kappa_{33}^f+\left(V^f\kappa_{33}^m\right)\right\}}{\left[(1-V^f)C_{22}^f+V^f C_{22}^m\right]\left[(1-V^f)C_{55}^f+V^f C_{55}^m\right]\left[(1-V^f)\kappa_{11}^f+V^f\kappa_{11}^m\right]}
\end{aligned}
$$

6. Appendix - B

$$
\begin{aligned}
S^3 &= A_1\left(1-V^f\right)\left(C_{13}^m-C_{13}^f\right)+B_1\left(1-V^f\right)\left(C_{23}^m-C_{23}^f\right)+\left(C_1\left(1-V^f\right)e_{13}^m\right)\\
K^3 &= B_1\left(1-V^f\right)\left(C_{13}^m-C_{13}^f\right)+J_1\left(1-V^f\right)\left(C_{23}^m-C_{23}^f\right)-\left(D_1\left(1-V^f\right)e_{13}^m\right)\\
M^3 &= K_1\left(1-V^f\right)\left(C_{13}^m-C_{13}^f\right)+M_1\left(1-V^f\right)\left(C_{23}^m-C_{23}^f\right)-\left(P_1\left(1-V^f\right)e_{13}^m\right)\\
S^6 &= \left(A_1\left(1-V^f\right)e_{31}^f\right)+\left(B_1\left(1-V^f\right)e_{32}^f\right)-\left(K_1\left(1-V^f\right)e_{35}^m\right)\\
K^6 &= \left(B_1\left(1-V^f\right)e_{31}^f\right)+\left(J_1\left(1-V^f\right)e_{32}^f\right)-\left(M_1\left(1-V^f\right)e_{35}^m\right)\\
F^3 &= -C_1(1-V^f)\left(C_{13}^m-C_{13}^f\right)+D_1(1-V^f)\left(C_{23}^m-C_{23}^f\right)+\left(H_1(1-V^f)e_{13}^m\right)\\
F^7 &= -C_1(1-V^f)\left(\beta_{11}^m-\beta_{11}^f\right)+D_1(1-V^f)\left(\beta_{22}^m-\beta_{22}^f\right)+H_1(1-V^f)\left(P_1^m-P_1^f\right)\\
M^6 &= \left(K_1\left(1-V^f\right)e_{31}^f\right)+\left(M_1\left(1-V^f\right)e_{32}^f\right)-\left(N_1\left(1-V^f\right)e_{35}^m\right)\\
S^7 &= A_1\left(1-V^f\right)\left(\beta_{11}^m-\beta_{11}^f\right)+B_1\left(1-V^f\right)\left(\beta_{22}^m-\beta_{22}^f\right)+C_1\left(1-V^f\right)\left(P_1^m-P_1^f\right)\\
K^7 &= B_1\left(1-V^f\right)\left(\beta_{11}^m-\beta_{11}^f\right)+J_1\left(1-V^f\right)\left(\beta_{22}^m-\beta_{22}^f\right)-D_1\left(1-V^f\right)\left(P_1^m-P_1^f\right)\\
A_{11} &= \left((1-V^f)C_{44}^f+V^fC_{44}^m\right)\left((1-V^f)\kappa_{22}^f+V^f\kappa_{22}^m\right)+\left((1-V^f)e_{24}^f\right)\times\\
&\quad \left((1-V^f)C_{55}^f+V^fC_{55}^m\right)\\
A_0 &= \left((1-V^f)C_{55}^f+V^fC_{55}^m\right)\left(1-V^f)C_{11}^f+V^fC_{11}^m\right)\left(1-V^f)\kappa_{11}^f+V^f\kappa_{11}^m\right)\times\\
&\quad \left(1-V^f)C_{22}^f+V^fC_{22}^m\right)\\
A_1 &= \frac{A_{11}\left[((1-V^f)e_{24}^f)^2\left((1-V^f)C_{22}^f+V^fC_{22}^m\right)+\left((1-V^f)C_{55}^f+V^fC_{55}^m\right)\left(V^fe_{12}^m\right)^2\right]}{A_0}\\
B_1 &= \frac{A_{11}\left[((1-V^f)e_{24}^f)^2\left((1-V^f)C_{12}^f+V^fC_{12}^m\right)+\left((1-V^f)C_{55}^f+V^fC_{55}^m\right)\left(V^fe_{12}^m\right)^2\right]}{A_0}\\
C_1 &= \frac{A_{11}\left[((1-V^f)e_{24}^f)^2\left((1-V^f)\kappa_{22}^f+V^f\kappa_{22}^m\right)+\left((1-V^f)C_{55}^f+V^fC_{55}^m\right)\left(V^fe_{12}^m\right)^2\right]}{A_0}\\
D_1 &= \frac{A_{11}\left[((1-V^f)e_{24}^f)^2\left((1-V^f)\kappa_{22}^f+V^f\kappa_{22}^m\right)+\left((1-V^f)C_{11}^f+V^fC_{11}^m\right)\left(V^fe_{12}^m\right)^2\right]}{A_0}\\
J_1 &= \frac{A_{11}\left[((1-V^f)e_{24}^f)^2\left((1-V^f)\kappa_{22}^f+V^f\kappa_{22}^m\right)+\left((1-V^f)e_{24}^f+V^fe_{24}^m\right)\left(V^fe_{11}^m\right)^2\right]}{A_0}\\
K_1 &= \frac{A_{11}\left[((1-V^f)C_{44}^f)^2\left((1-V^f)\kappa_{22}^f+V^f\kappa_{22}^m\right)+\left((1-V^f)C_{55}^f+V^fC_{55}^m\right)\left(V^fe_{12}^m\right)^2\right]}{A_0}\\
M_1 &= \frac{A_{11}\left[((1-V^f)C_{44}^f)^2\left((1-V^f)\kappa_{22}^f+V^f\kappa_{22}^m\right)+\left((1-V^f)C_{11}^f+V^fC_{11}^m\right)\left(V^fC_{12}^m\right)^2\right]}{A_0}\\
N_1 &= \frac{A_{11}\left[((1-V^f)C_{44}^f)^2\left((1-V^f)\kappa_{22}^f+V^f\kappa_{22}^m\right)+\left((1-V^f)e_{12}^f+V^fe_{12}^m\right)\left(V^fe_{11}^m\right)^2\right]}{A_0}\\
H_1 &= \frac{A_{11}\left[((1-V^f)C_{44}^f)^2\left((1-V^f)\kappa_{22}^f+V^f\kappa_{22}^m\right)+\left((1-V^f)e_{12}^f+V^fe_{12}^m\right)\left(V^fe_{11}^m\right)^2\right]}{A_0}\\
P_1 &= \frac{A_{11}\left[((1-V^f)C_{44}^f)^2\left((1-V^f)\kappa_{22}^f+V^f\kappa_{22}^m\right)+\left((1-V^f)e_{24}^f+V^fe_{24}^m\right)\left(V^fC_{12}^m\right)^2\right]}{A_0}
\end{aligned}
\tag{10}
$$

References

Avellaneda, M. and Swart, P. (1994). Calculating the performance of 1-3 piezocomposites for hydrophone applications: an effective medium approach. *J. Acoust. Soc. Am.* **103**, pp. 1449–1467.

Avellaneda, M. and Swart, P. (1998). Calculating the performance of 1-3 piezocomposites for hydrophone applications:an effective medium approach, *J. Acoust. Soc. Am.* **103**, pp. 1449–1467.

Barnett, D. and Lothe, J. (1997). Dislocations and line charges in anisotropic piezoelectric insulators, *Phys. Status Solid-B* **67**, pp. 105–111.

Berger, H., Kari, S., Gabbert, U., Rodriguez-Ramos, R., Bravo-Castillero, J. and Guinovart-Diaz, R. (2007). Evaluation of effective material properties of randomly distributed short cylindrical fiber composites using a numerical homogenization technique, *J. Mech. Mater. Struct.* **2**, pp. 1561–1570.

Della, C. N. and Shu, D. (2008). The performance of 1-3 piezoelectric composites with a porous non-piezoelectric matrix, *Acta Mater.* **56**, pp. 754–761.

Dunn, M. and Taya, M. (1993). Micromechanics predictions of the effective electroelastic moduli of piezoelectric composites, *Int. J. Solids Struct.* **30**, pp. 161–175.

Hull, D. and Clyne, T. (1996). *An introduction to composite* (Cambridge University Press, New York).

Kar-Gupta, R. and Venkatesh, T. (2007). Electromechanical response of 1-3 piezoelectric composites: An analytical model, *Acta Mater.* **55**, pp. 1093–1108.

Klicker, K., Biggers, J. and Newnham, R. (1981). Composite of pzt and epoxy for hydrostatic transducers application, *J. Amer. Ceramic Soc.* **64**, pp. 5–9.

Kumar, A. and Chakraborty, D. (2009). Effective properties of thermo-electro-mechanically coupled piezoelectric fiber reinforced composites, *Mat. Design* **30**, pp. 1216–1222.

Nan, C., Liu, L., Guo, D. and Li, L. (2000). Calculations of the effective properties of 13 type piezoelectric composites with various rod/fibre orientations, *J. Phys. D: Appl. Phys.* **33**, pp. 2977–2984.

Nelson, L. (2002). Smart piezoelectric fibre composites, *Mater. Sci. Tech.* **18**, pp. 1245–1256.

Newnham, R., Skinner, D. and Cross, L. (1978). Connectivity and piezoelectric-pyroelectric composites, *Mat. Res. Bull.* **13**, pp. 525–536.

Odegard, G. (2004). Constitutive modeling of piezoelectric polymer composites, *Acta Mater.* **52**, pp. 5315–5330.

Pettermann, H. and Suresh, S. (2005). A comprehensive unit cell model: a study of coupled effects in piezoelectric 1-3 composites, *Int. J. Solids Struct.* **37**, pp. 5447–5464.

Poizat, C. and Sester, M. (1999). Effective properties of composites with embedded piezoelectric fibres, *Comput. Mater. Sci.* **16**, pp. 89–97.

Sakthivel, M. and Arockiarajan, A. (2010). An analytical model for predicting thermo-electro-mechanical response of 1-3 piezoelectric composites, *Comput. Mater. Sci.* **48**, pp. 759–767.

Srihari, D. (2011). Analytical and numerical studies on effective properties of piezocomposites, *Masters Thesis, IIT Madras* **44**, pp. 673–677.

Tauchert, T. (1992). Piezothermoelastic behavior of a laminated plate, *J. Thermal Stresses* **15**, pp. 25–37.

Taunaumang, H., Guy, I. L. and Chan, H. L. W. (1994). Electromechanical properties of 1-3 piezoelectric ceramic/piezoelectric polymer composites, *J. Appl. Phys.* **76**, pp. 484–489.

Topolov, V. and Bowen, C. (2009). *Electromechanical properties in composites based on ferroelectrics* (Springer, London).

Uchino, K. (2000). *Ferroelectric devices* (Marcel Dekker Inc., New york).